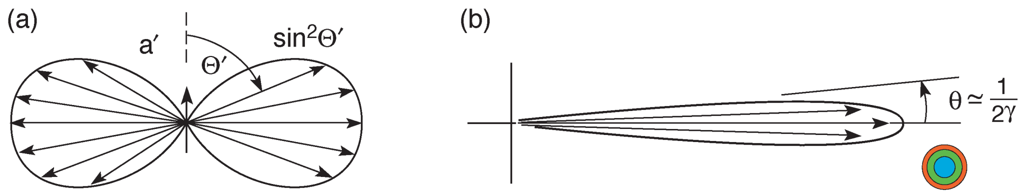

COLORPLATE VI. (a) Illustration of the radiation pattern of an oscillating electron in the frame of reference moving with the average electron speed. (b) Illustration of the radiation pattern of a highly relativistic electron as observed in the laboratory frame of reference. The shortest wavelengths are observed on axis. (Following Hofmann.) See text, p. 138.

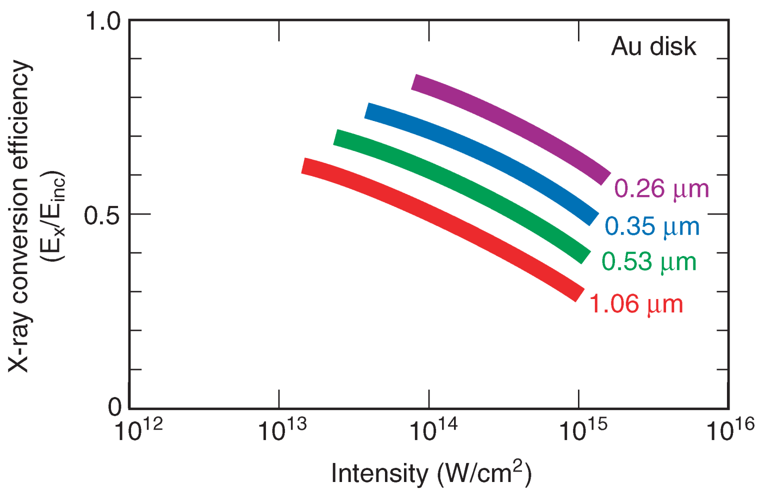

COLORPLATE VII. Curves showing the trend of x-ray conversion energy within the broad 0.1 keV to 1.5 keV spectral window, divided by the incident laser energy, assuming a Lambertian ($\cos\theta$) angular distribution in the emission hemisphere. Efficiency is shown as a function of intensity for Nd laser light at 1.06 μm (red) and its harmonics at 0.53 μm (green), 0.35 μm (blue), and 0.26 μm (ultraviolet) for nanosecond duration pulses. The target is a gold disk. The curves are derived largely from the data of R. Kauffman, H. Kornblum, G. Tirsell, P. Lee, R. Turner, and colleagues, Lawrence Livermore National Laboratory. See text, p. 258.

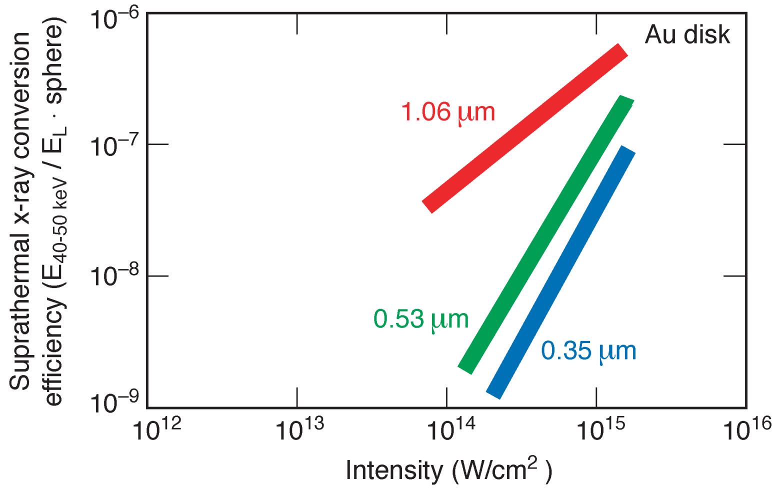

COLORPLATE VIII. Curves showing the general trend of suprathermal x-ray generation vs. laser intensity and wavelength. The specific data here shows radiated energy in a 40–50 keV spectral window, as a function of incident laser intensity for three wavelengths: 1.06 μm (red), 0.53 μm (green), and 0.35 μm (blue). The curves are derived from the data of E.M. Campbell, B. Pruett, R. Turner, F. Ze, and W. Mead, LLNL. See text, p. 259.

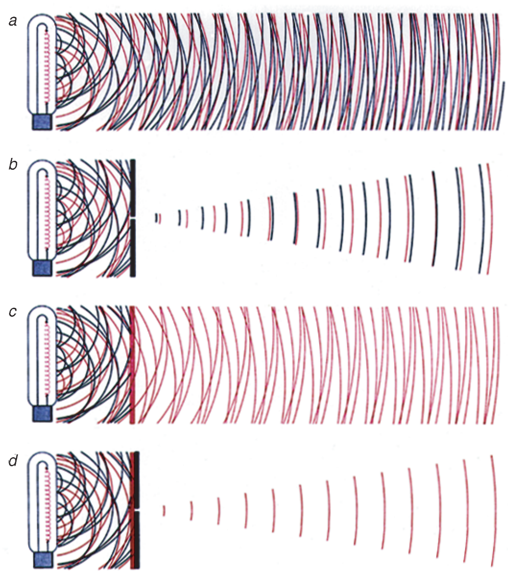

COLORPLATE IX. Spatial and spectral filtering is illustrated as a procedure to produce coherent radiation, albeit at greatly diminished power, from an ordinary thermal source of visible light. In the nomenclature used here, d would be the diameter of the pinhole shown in part (d), and θ would be the divergence half angle in part (d), set either by the radiation emission characteristics, by a downstream acceptance aperture, or by a lens. (Courtesy of A. Schawlow, Stanford.) See text, p. 309.